

An Extensive, Sensitive Search for SiO Masers in High- and Intermediate-Mass Star-Forming Regions

Luis A. Zapata¹, Karl Menten¹, Mark Reid² and Henrik Beuther³

Received _____; accepted _____

¹Max-Planck-Institut für Radioastronomie, Auf dem Hügel 69, 53121 Bonn, Germany

lzapata, kmenten@mipfr-bonn.mpg.de

²Harvard-Smithsonian Center for Astrophysics, 60 Garden Street, MS-42, Cambridge, MA 02138 USA

reid@cfa.harvard.edu

³Max-Planck-Institut für Astronomie, Königstuhl 17, 69117 Heidelberg, Germany

beuther@mpia-hd.mpg.de

ABSTRACT

We present sensitive Very Large Array observations with an angular resolution of a few arcseconds of the $J = 1 - 0$ line of SiO in the $v=1$ and 2 vibrationally excited states toward a sample of 60 Galactic regions in which stars of high or intermediate mass are currently forming and/or have recently formed. We report the detection of SiO maser emission in *both* vibrationally excited transitions toward only three very luminous regions: Orion-KL, W51N and Sgr B2(M). Toward all three, SiO maser emission had previously been reported, in Orion-KL in both lines, in W51N only in the $v = 2$ line and in Sgr B2(M) only in the $v = 1$ line. Our work confirms that SiO maser emission in star-forming regions is a rare phenomenon, indeed, that requires special, probably extreme, physical and chemical conditions not commonly found. In addition to this SiO maser survey, we also present images of the simultaneously observed 7 mm continuum emission from a subset of our sample of star-forming regions where such emission was detected. This is in most cases likely to be free-free emission from compact- and ultracompact-HII regions.

Subject headings: techniques: interferometric — techniques: spectroscopic — ISM: molecules — radio continuum: ISM — radio lines: ISM

1. INTRODUCTION – HISTORY AND MOTIVATION

SiO maser emission has been detected toward more than a thousand asymptotic giant branch (AGB) stars and a few red supergiants (RSGs; see, e.g., Benson et al. 1990; Habing 1996). These objects have luminosities larger than a few thousand of L_{\odot} (AGB stars) to $> 10^5 L_{\odot}$ (RSGs), which are comparable to the luminosities of intermediate- and high-mass protostellar and young stellar objects. Nevertheless, toward forming and young stars SiO maser emission seems to be very rarely observable.

Orion Kleinmann-Low (Orion-KL) was the first source in the sky toward which SiO maser emission was found (in the $v = 1, J = 2 - 1$ line) by Snyder & Buhl (1974). Subsequently, the first detections of the $J = 1 - 0$ line in the $v = 1$ and 2 states, also toward, among others, Orion-KL, were made by Thaddeus et al. (1974) and by Buhl et al. (1974), respectively. Toward the Orion-KL region, maser emission was also found in other SiO lines ($v = 1, J = 3 - 2$, Davis et al. 1974), including transitions from the vibrational ground state (Tsuboi et al. 1996), but, at least to our knowledge, not from states with $v > 2$, contrary to M-type stars. Moreover, maser lines from the ^{29}SiO and ^{30}SiO isotopomers (Olofsson et al. 1981), and even the very rare $^{28}\text{Si}^{18}\text{O}$ were found (Cho et al. 2005). Never detected, however, was the $v = 2, J = 2 - 1$ line. The latter line also remains undetected in oxygen-rich (M-type) evolved stars, although it is found in S-type stars (in which O and C abundances are equal). This behavior is explainable by the line’s pumping mechanism (Olofsson et al. 1981). Since the discovery of SiO maser emission in the Orion-KL region (Snyder & Buhl 1974), only two more high mass star-forming regions, W51N (= W51-IRS2) and Sgr B2(M) (Hasegawa et al. 1986; Ukita et al. 1987) have been found to show this kind of emission.

In the past, a number of surveys have been undertaken with the goal of finding SiO masers in a larger number of star-forming regions. The number of sources surveyed for

which upper limits have been published is less than two dozen and these upper limits are in the several Jy range (Jewell et al. 1985; Barvainis & Clemens 1984), barely sensitive enough to potentially detect the W51N maser, and much too shallow to detect the ~ 1 Jansky-strength maser in Sgr B2(M) (Hasegawa et al. 1986; Ukita et al. 1987).

Around luminous AGB stars/RSGs, SiO maser emission arises from a region of density around a few times 10^8 and 10^9 cm^{-3} and temperature above 1000 K, which is within a few stellar radii of the photosphere (Lockett & Elitzur 1992; Bujarrabal 1994). Given these extreme requirements, one expects this emission to pinpoint in star-forming regions the *exact* location of the embedded high-mass protostar that is exciting it, which frequently is not easy to determine by other means (see discussion in Menten & Reid 1995). This is certainly borne out by the best-studied SiO maser associated with a star formation region, that in Orion-KL. Menten & Reid (1995), using simultaneous high resolution VLA observations of the 43.2 GHz Orion-KL SiO maser and weak continuum emission (from source-I), which they accurately register with a $3.8 \mu\text{m}$ speckle image, clearly showed that at the position of “source-I” no infrared source is detected. Thus, all that is observed at infrared wavelengths (*i.e.* the famous IRc2) is reprocessed radiation, while the position of the continuum emission, which almost certainly comes from an ionized disk surrounding the protostar, is right at the center of the SiO maser distribution (Reid et al. 2007). While source-I clearly is self-luminous, as argued by Reid et al. (2007), it is unlikely to contribute a significant fraction of $\sim 10^5 L_{\odot}$ of the KL region.

The SiO maser in W51N seems to be different from that in Orion-KL, since it only appeared to show maser emission in the 42.8 GHz $v = 2, J = 1 - 0$ line, while that in Orion-KL shows emission in the $v = 1$ and 2 lines at comparable intensities. Morita et al. (1992) located the W51N SiO maser in a dense compact molecular core mapped in NH_3 emission by Ho et al. (1983) and Zhang & Ho (1997). Very Long Baseline Array (VLBA)

radio observations by Eisner et al. (2002) reveal a comparable linear extent to that observed in Orion-KL. It is clear from the latter data that, while H₂O masers (also imaged by Eisner et al. 2002) trace a highly luminous region on a few arcsecond (few tenths of a parsec) scales, only the SiO maser marks, as in Orion, the exact location of a self-luminous power source.

Sub-milliarcsecond resolution VLBA observations show that the W51N SiO masers may be tracing the limbs of an accelerating bipolar outflow close to the “*dominant center*” (where are located most of the H₂O, OH and SiO masers) (Eisner et al. 2002). No radio continuum emission is detected toward this SiO maser. However, the radio emission from Source-I would be completely undetectable at the distance of W51 (~ 7 kpc).

Finally, little is known about the Sgr B2(M) SiO maser, from which only the $v = 1$ line had been found, except for the fact that it is located close to (but not coincident with) the radio source F, which at high resolution splits into several compact sub-sources (Gaume et al. 1995). As in W51N, the SiO maser is close to a compact clump of NH₃ emission imaged by Vogel et al. (1987).

In this work, we present a sensitive search for SiO maser emission toward a sample of 60 high-mass star-forming regions using the Very Large Array. We report the detection of such emission in *both* vibrationally excited transitions ($v=1$ and 2) and *only* toward Orion-KL, W51N, and Sgr B2(M). This suggests that SiO maser emission is indeed a very special physical phenomenon possibly only occurring within a short time period during the formation of high-mass stars. Simultaneously, we obtained moderate sensitivity data of those sources at 7 mm.

In §2 we introduce our sample and in §3 discuss the observations undertaken in this study. In §4 we present and discuss our SiO data and also our 7 mm continuum data.

2. THE SAMPLE

The 60 massive star-forming regions observed were selected from the sample of 69 high-mass protostellar objects of Sridharan et al. (2002) and the classical sample of mid-infrared selected star-forming regions studied by Willner et al. (1982). The luminosities of these sources mostly range from several times 10^3 to a few times $10^5 L_{\odot}$, which is comparable to the range from Mira variable to the RSG that are commonly found in the host stars of strong SiO masers. We note that the luminosities of the SiO masers in the supergiants, *i. e.* VX Sgr or VY CMa, are typically 1 or 2 orders higher than those of Miras and comparable or even higher than those of the Orion-KL SiO maser. In Table 1, we summarize the main properties of the 60 objects selected.

3. OBSERVATIONS

The observations were made with the NRAO¹ Very Large Array (VLA) between 2003 April 14 and May 1. Two intermediate frequency (IF) bands were employed: one detecting right circular polarization, centered at 42.820555 GHz, the rest frequency of the $J = 1 - 0, v = 2$ ²⁸SiO line; the other, detecting left circular polarization, was centered at 43.122039 GHz, the rest frequency of the $J = 1 - 0, v = 1$ ²⁸SiO line. These rest frequencies were calculated using the high accuracy molecular constants determined by Molla et al. (1991).

Both IF bands of the VLA correlator were configured in line mode with 32 channels covering 12.5 MHz, which provided 391 kHz (2.72 km s^{-1}) resolution.

¹The National Radio Astronomy Observatory is a facility of the National Science Foundation operated under cooperative agreement by Associated Universities, Inc.

The integration time on each source was about 5 minutes. At this epoch, the VLA was in its D configuration. The absolute flux density calibrator was 1331+305, for which we adopted a flux density of 1.47 Jy. Amplitudes and phases were calibrated by observations of compact extragalactic radio sources close in position to our program sources. In Table 2, we present the list of the compact extragalactic radio sources used as secondary calibrators and their bootstrapped flux densities.

The data were edited and calibrated in the standard manner using the software packages AIPS and MIRIAD developed by the NRAO and BIMA². Maps were obtained using the AIPS task IMAGR and the MIRIAD tasks INVERT, CLEAN, and RESTORE. For sources free of line emission, continuum maps were produced from “*channel 0*” data, *i.e.*, pseudo-continuum (u, v) -databases containing the inner 75% of the bandpass. For the sources showing maser emission, the (u, v) -data channels free of line emission and not affected by band edge were averaged and imaged. For most of the 7 mm continuum maps, we used the ROBUST weighting parameter set to 0, for an optimal compromise between sensitivity and angular resolution. However, for fainter sources we use ROBUST=5, which corresponds to natural weighting, to achieve maximum sensitivity in each continuum image. Finally, the strongest 7 mm continuum sources were self-calibrated in phase and amplitude. The resulting *rms* noise of the line images was better than about 10 mJy beam⁻¹ per channel. In a few sources, it was higher due to unfavorable weather conditions and/or low declinations. The results of the continuum imaging are discussed in §4.4.

²The Berkeley Illinois Maryland Association

4. RESULTS AND DISCUSSION

4.1. The SiO Maser Emission

In Table 1, we present the main results of our search for SiO masers in both vibrationally excited ($v=1$ and 2) transitions toward the 60 high- and intermediate-mass star forming regions. We detected SiO $J = 1 - 0$ maser emission in both the $v = 1$ and 2 lines above the $5\text{-}\sigma$ levels (or about 50 mJy) only toward Orion-KL, W51N, and Sgr B2(M).

4.2. Source-I

The SiO maser emission from both vibrationally excited transitions associated with Orion-KL shows its characteristic double-peak profile centered near 6 km s^{-1} (the systemic velocity of the molecular cloud core, see Figure 1). As already found in many previous studies dating back to Snyder & Buhl (1974), two groups of features are observed, in the $[-14, +3] \text{ km s}^{-1}$ and $[+8, 23] \text{ km s}^{-1}$ intervals, with little emission in between.

It is interesting to note that the flux density of the SiO maser emission toward the sources Sgr B2(M) and Orion-KL in the $v=1$ vibrationally excited transition is stronger than that in the $v=2$ transition, while in W51N the reverse is true (see Figure 1).

Finally, comparing the flux densities of the SiO maser emission in the Orion-KL, W51N and Sgr B2(M), we have calculated that the SiO masers in Orion-KL are approximately one order of magnitude more luminous than those in W51N and Sgr B2(M) (see Table 3).

4.2.1. *The Nature of the SiO Emission*

The SiO maser emission toward high-mass star forming regions has been associated with powerful bipolar protostellar outflows (Greenhill et al. 1998; Eisner et al. 2002). VLBA radio observations (with ~ 1 mas resolution) of the Orion-KL SiO masers were consistent with an origin in a wide-angle biconical flow (with a “X”-like pattern) with the SiO masers outlining the limbs of the outflow cavity and centered on the source-I (Greenhill et al. 1998). More recent data, however, suggests that the SiO masers originate in the material expelled from a rotating disk around “source I” (Greenhill et al. 2004; Reid et al. 2007).

4.3. **W51N, Sgr B2(M), and Source-I**

We found SiO $J = 1 - 0$ maser emission in *both* vibrationally excited transitions toward W51N and Sgr B2(M) (see Figure 1).

Toward Sgr B2(M) the $v=1$ SiO maser emission shows a single peak that is redshifted from the cloud systemic velocity (about 60 km s^{-1}), has a linewidth of about 13 km s^{-1} and is centered at a v_{LSR} of 87 km s^{-1} . The $v=2$ transition only shows one redshifted very narrow line centered at a v_{LSR} of 96 km s^{-1} . The latter line is unresolved with our 2.72 km s^{-1} resolution, and is atypically narrow for an SiO maser line. We are nevertheless convinced of its reality as the emission arises from the same position as the $v = 1$ emission.

Toward W51N the $v=1$ SiO maser line is spread over 12 km s^{-1} and is centered near $v_{LSR} = 50 \text{ km s}^{-1}$, close to the systemic velocity of the molecular cloud core associated with W51. The $v=2$ transition shows emission over 20 km s^{-1} , centered at a similar velocity of $v_{LSR} = 49 \text{ km s}^{-1}$. Neither lines exhibit a double peak appearance.

In the W51N region, the SiO maser emission is tracing a high velocity ($\sim 80 \text{ km s}^{-1}$) bipolar protostellar outflow with a size of about 10^4 AU that emanates from a molecular

core observed in NH_3 (Morita et al. 1992) as discussed before. We note that in the case of Sgr B2(M) the SiO maser emission only shows high velocity redshifted emission ($\sim 30 \text{ km s}^{-1}$) emanating from a molecular NH_3 core (Morita et al. 1992).

4.3.1. Variability

Toward two of our SiO maser associated with SFRs (Source-I and W51N) we see clear signs of variability, but only for Source-I do extensive monitoring data exist. Comparing the flux density of the SiO $v = 1, J = 1 - 0$ transition reported by Menten and Reid (1995) toward Source-I with that measured by us (Figure 1 and Table 3) we found a ~ 3 times lower value.

Long term monitoring of the Orion-KL $J = 1 - 0$ SiO maser lines generally shows the $v = 1$ line stronger than the $v = 2$ line (Martinez et al. 1988; Alcolea et al. 1999; Pardo et al. 2004) with the ratio varying between > 4 and < 2 . The ratio we measure (~ 2) is in line with this behavior and our flux densities are at the low end of the values found during the monitoring.

4.3.2. Comparison with Red Giant and Supergiant Stars

The long timerange monitoring of SiO $J = 1 - 0$ masers with the Yebes 14 m telescope (Martinez et al. 1988; Pardo et al. 2004) reveals that both the $v=1$ and the $v=2$ lines exhibit dramatic variability in some Mira stars. In α Ceti, for example, the SiO luminosity may vary by a factor > 500 over a 332 d variability cycle, with a maximum SiO luminosity near the same time as the infrared radiation. Higher luminosity/higher mass-loss RSGs show longer term SiO variability and higher SiO maser luminosities. Both SiO lines toward the supergiants VY CMa and VX Sgr show a long-term decline with a drop to half intensity

over ~ 1500 days, longer than the infrared variability cycles of these objects.

Towards μ Cep the intensity in both lines increased > 5 fold over an 800 day period and then declined by an even larger factor over a similar interval and has been at a low level for years. Finally, a number of well-known RSGs (e.g. α Ori, α Sco, and α Her) do not show any maser emission at all.

It is interesting to compare the luminosities of the SiO masers in SFR with the typical luminosity ranges of Mira and RSG SiO masers that we have added to Table 3. It looks like as if the SFR SiO maser luminosities are higher than the luminosities of Mira stars but lower than that of the RSGs. The same appears to be true for the luminosities of the exciting stars.

4.4. 7 mm Continuum Emission

Of the 60 massive star-forming regions observed in our survey, 7 mm continuum emission was only detected toward 17 above a $4\text{-}\sigma$ level. Continuum maps of these sources are shown in Figure 1 and flux densities and source sizes are given in Table 4. The continuum emission is most likely free-free emission from compact and ultracompact HII regions. However in a few sources, there are indications that it might originate from ionized jets, dusty envelopes and/or disks. In Table 5 we give a tentative interpretation for the nature of these sources, based mostly on other centimeter/millimeter continuum observations at high angular resolution and, in some cases, on their spectral energy distributions (SEDs).

We detected 14 ultracompact and compact H II regions: N6334I, Sgr B2(M), AFGL 2046, AFGL 2136, W51N, W51e1, W51e2, W51IRS1, AFGL 2591, NGC7538 IRS1-A, NGC7538-IRS1-B, W3 IRS5, W3(OH), and MonR2. For all of these sources, data taken at other wavelength have been reported earlier (see Table 5). The sources show three different

type of morphologies: cometary, unresolved, or irregular (see Figure 1), with the cometary morphology dominating.

It is interesting to note that out of 32 objects selected from the sample of high-mass protostellar objects of Sridharan et al. (2002), only one was detected at 7 mm (I18440–0148). This could be explained if these objects are young (proto)stars with no or very faint free-free emission (less than a few mJy) as selected by Sridharan et al. (2002). Dust emission at 7 mm wavelength is expected to be very faint and not detectable with our integration times. Moreover, Zapata et al. (2006) using observations of the VLA found that the 7 mm continuum emission from 10 massive dusty objects of this sample is less than a few mJy.

At a $4\text{-}\sigma$ level (> 2 mJy), we do not detect the arcsec-sized hypercompact HII regions located in the NGC7538 IRS9, W33A, and AFGL 2591 and that one reported by van der Tak & Menten (2005) toward W3IRS5. Neither do we detect source-I in Orion, the continuum source associated with the SiO masers (Menten & Reid 1995; Reid et al. 2007). Note, however, that the noise level in our Orion continuum image is particularly high, mainly as our bandwidth provided not enough channels free of line emission to make the continuum image. Also, we do detect the hypercompact HII region RS4 discussed by Menten & van der Tak (2004). Finally, we note that the continuum flux density at this wavelength for W3(OH) is low compared to those fluxes reported at 1.3 cm and 3 mm by Wilner et al. (1995); Wilson et al. (1991). It could be explained if the source is variable in time as reported at 1.3 cm by Guilloteau et al. (1983).

4.4.1. *Comments on Selected Individual Sources*

Sgr B2(M)

As shown in Figure 2, we found two strong 7 mm continuum sources in Sgr B2(M) (A in the west and B in the east). These two sources are the counterpart of the compact objects F1–F4 and the compact HII region “I” reported by Gaume et al. (1995) at 1.3 cm, but due to our poor angular resolution ($\sim 5'' \times 1''$ at P.A.=150°) we could not resolved them.

The F1–F4 objects have been already imaged at 7 mm with much higher angular resolution ($0''.06$), with the VLA (de Pree et al. 1998) and were resolved into a total of ~ 20 separate HC HII regions.

Kuan et al. (1996) have compiled continuum flux densities for Sgr B2(M) at frequencies between 4.9 to 8.3 GHz and between 78.5 to 109.9 GHz. Our 43 GHz observations bridge an important frequency gap, and the total flux density we measure for Sgr B2(M) indicates a fairly flat spectrum with dust only contributing significantly at higher frequencies. While the numerous UC HII regions present in Sgr B2(M) are expected to have rising or falling spectra, the effective spectral index is likely the result of more extended (flatter spectral index) emission dominating the integrated emission analyzed by Kuan et al. (1996) and us.

I18440–0148

I18440–0148 was the only one from the sample of Sridharan et al. (2002) detected at 7 mm. From the 3.6 cm continuum flux ≤ 1 mJy (Sridharan et al. 2002) and the 7 mm flux measured by us (see Table 4), we calculated a spectral index of $\alpha \geq 1.1$. We, thus, suggest that the 7 mm continuum emission of this source is moderately optically thick free-free emission from an ultra-compact HII region.

DR21(OH)

DR21(OH) (or W75S) is a very young high mass star forming region with a bolometric luminosity of $1 \times 10^3 L_{\odot}$ showing very faint centimeter continuum emission (Argon et al. 2000). It also shows strong compact millimeter continuum emission (Woody et al. 1989; Padin et al. 1989) and H₂O, OH and class I as well as class II CH₃OH maser emission (Argon et al. 2000; Mangum et al. 1992; Plambeck & Menten 1990; Menten 1991). Class I CH₃OH masers trace a powerful east-west bipolar outflow almost perpendicular to the plane of sky Kogan & Slysh (1998). Toward this region we detect a compact source that is the 7 mm counterpart of the millimeter source MM1 (Woody et al. 1989; Padin et al. 1989). This source is found to be resolved at this wavelength (see Table 4).

From the 3.6 cm continuum peak flux density value (~ 0.31 mJy) reported by Argon et al. (2000) of this region and our 7 mm value (Table 4), we calculate a spectral index of $\alpha=1.98\pm 0.2$ that suggests that its cm continuum emission maybe optically-thick free-free emission from a ultra-compact HII region. However, if we take the 2.7 mm continuum flux density (~ 0.3 Jy) reported by Woody et al. (1989) for MM1, we find a much steeper spectral index of $\alpha=3.6\pm 0.4$, very close to that derived by Woody et al. (1989) from the 1.4 and 2.7 mm continuum measurements. We think that the emission at 7 mm might be partially optically thin dust emission from either a dusty envelope or disk, or both.

AFGL 490

The AFGL 490 region is located at about 1 kpc distance (Snell et al. 1984), has a mass of $490 M_{\odot}$, a bolometric luminosity of $2 \times 10^3 L_{\odot}$ and is still embedded in its parent molecular cloud ($A_V \sim 40$ mag, Alonso-Costa & Kwan 1989). Its central object drives a high-velocity outflow (Mitchell et al. 1995). Very recently Schreyer et al. (2006) by using ¹⁷CO line and

1.3 mm continuum observations with an angular resolution of about $1''$ found evidence of rotating dusty disk driving the molecular outflow.

In this region we found a compact (~ 2000 AU size) source that is the 7 mm counterpart of the millimeter source reported by Schreyer et al. (2006).

AFGL 961

AFGL 961 is also a relatively close-by high-mass star forming region with a bolometric luminosity of about $10^4 L_{\odot}$. This region is composed of two near-IR objects (E and W), separated by about $5''$ (8000 AU). Castelaz et al. (1985) show that the spectral energy distribution of GL 961-E dominates at wavelengths longer than $2.2 \mu\text{m}$, while the western object is brighter at shorter wavelengths. This binary system is located at the center of a parsec scale molecular outflow oriented in the N-S direction with the approaching lobe towards the north (Lada & Gautier 1982). Very recently Alvarez et al. (2004) found a third faint infrared object associated with the western source.

We found a faint and unresolved 7 mm continuum source that is the millimeter counterpart of the infrared source GL 961-E. Single-dish (sub)millimeter 350, 870, and 1300 μm data all taken with beam sizes of $30''$ or larger cannot discriminate between AFGL 961W and E (Guertler et al. 1991). If we *assume* that all the (sub)millimeter flux and the radio emission arise from the same source (AFGL 961E) we can construct the SED, shown in Figure 3. It shows a spectrum in which the emission is dominated by a component that rises rapidly with frequency with a spectral index of $\alpha = 3.0$. A simple interpretation would be that the 7 mm continuum emission from GL 961-E is associated with dust emission from a core or disk. Clearly, however, more high resolution radio and (sub)mm observations are needed to test this interpretation.

5. SUMMARY

We report the detection of SiO maser emission in *both* vibrationally excited transitions from massive star forming regions only towards three very luminous regions (Orion-KL, W51N and SgrB2(M)) out of the 60 observed galactic star-forming regions. Toward all three, SiO maser emission had previously been reported, in Orion-KL in both lines, in W51N only in the $v = 2$ line and in Sgr B2(M) only in the $v = 1$ line. Since we do not detect either SiO line in 57 other regions of intermediate- and high-mass star formation, our work confirms that such emission in star-forming regions is a rare phenomenon, indeed, that requires special, probably extreme, physical and chemical conditions not commonly found. In addition to this SiO data, we also present images of the simultaneously observed 7 mm continuum emission from a subset of our sample of star-forming regions where such emission was detected. This is in most cases likely to be free-free emission from compact- and ultracompact-HII regions.

We thank the anonymous referee for many valuable suggestions. This research has made extensive use of the SIMBAD database, operated at CDS, Strasbourg, France, and NASA’s Astrophysics Data System.

REFERENCES

- Alcolea, J. et al. 1999, *A&AS*, 139, 461
- Alonso-Costa, J. L., & Kwan, J. 1989, *ApJ*, 338, 403
- Alvarez, C., Hoare, M., Glindemann, A., & Richichi, A. 2004, *A&A*, 427, 505, arXiv:astro-ph/0407079
- Alvarez, C., & Hoare, M. G. 2005, *A&A*, 440, 569
- Argon, A. L., Reid, M. J., & Menten, K. M. 2000, *ApJS*, 129, 159
- Barvainis, R., & Clemens, D. P. 1984, *AJ*, 89, 1833
- Benson, P. J., Little-Marenin, I. R., Woods, T. C., Attridge, J. M., Blais, K. A., Rudolph, D. B., Rubiera, M. E., & Keefe, H. L. 1990, *ApJS*, 74, 911
- Beuther, H., Schilke, P., Menten, K. M., Motte, F., Sridharan, T. K., & Wyrowski, F. 2002, *ApJ*, 566, 945, astro-ph/0110370
- Boonman, A. M. S., & van Dishoeck, E. F. 2003, *A&A*, 403, 1003
- Buhl, D., Snyder, L. E., Lovas, F. J., & Johnson, D. R. 1974, *ApJ*, 192, L97+
- Bujarrabal, V. 1994, *A&A*, 285, 953
- Carral, P., Kurtz, S. E., Rodríguez, L. F., Menten, K., Cantó, J., & Arceo, R. 2002, *AJ*, 123, 2574
- Chini, R., Henning, T., & Pfau, W. 1991, *A&A*, 247, 157
- Cho, S.-H., Kim, H.-G., Park, Y.-S., Choi, C.-H., & Ukita, N. 2005, *ApJ*, 622, 390
- Crampton, D., Georgelin, Y. M., & Georgelin, Y. P. 1978, *A&A*, 66, 1

- Davis, J. H., Blair, G. N., van Till, H., & Thaddeus, P. 1974, *ApJ*, 190, L117+
- de Pree, C. G., Gaume, R. A., Goss, W. M., & Claussen, M. J. 1996, *ApJ*, 464, 788
- de Pree, C. G., Goss, W. M., & Gaume, R. A. 1998, *ApJ*, 500, 847
- de Vicente, P., Martín-Pintado, J., Neri, R., & Colom, P. 2000, *A&A*, 361, 1058,
astro-ph/0009195
- Eisner, J. A., Greenhill, L. J., Herrnstein, J. R., Moran, J. M., & Menten, K. M. 2002, *ApJ*,
569, 334, astro-ph/0112093
- Erickson, E. F., & Tokunaga, A. T. 1980, *ApJ*, 238, 596
- Franco-Hernández, R., & Rodríguez, L. F. 2004, *ApJ*, 604, L105, arXiv:astro-ph/0402467
- Gaume, R. A., Claussen, M. J., de Pree, C. G., Goss, W. M., & Mehringer, D. M. 1995,
ApJ, 449, 663
- Gaume, R. A., Johnston, K. J., & Wilson, T. L. 1993, *ApJ*, 417, 645
- Gómez, Y., Rodríguez, L. F., Garay, G., & Moran, J. M. 1991, *ApJ*, 377, 519
- Greenhill, L. J., Gwinn, C. R., Schwartz, C., Moran, J. M., & Diamond, P. J. 1998, *Nature*,
396, 650, astro-ph/9811318
- Greenhill, L. J., Reid, M. J., Chandler, C. J., Diamond, P. J., & Elitzur, M. 2004, in *IAU
Symposium*, ed. M. Burton, R. Jayawardhana, & T. Bourke, 155–+
- Guertler, J., Henning, T., Kruegel, E., & Chini, R. 1991, *A&A*, 252, 801
- Guilloteau, S., Stier, M. T., & Downes, D. 1983, *A&A*, 126, 10
- Habing, H. J. 1996, *A&A Rev.*, 7, 97

- Hasegawa, T., Morita, K., Okumura, S., Kaifu, N., Suzuki, H., Ohishi, M., Hayashi, M., & Ukita, N. 1986, in *Masers, Molecules, and Mass Outflows in Star Formation Regions*, 275–+
- Henning, T., Pfau, W., & Altenhoff, W. J. 1990, *A&A*, 227, 542
- Ho, P. T. P., Das, A., & Genzel, R. 1983, *ApJ*, 266, 596
- Hoare, M. G. 2002, in *ASP Conf. Ser. 267: Hot Star Workshop III: The Earliest Phases of Massive Star Birth*, ed. P. Crowther, 137–+
- Hoare, M. G. 2006, *ApJ*, 649, 856, [astro-ph/0605662](#)
- Humphreys, R. M. 1978, *ApJS*, 38, 309
- Jewell, P. R., Walmsley, C. M., Wilson, T. L., & Snyder, L. E. 1985, *ApJ*, 298, L55
- Klein, R., Posselt, B., Schreyer, K., Forbrich, J., & Henning, T. 2005, *ApJS*, 161, 361, [astro-ph/0508191](#)
- Kogan, L., & Slysh, V. 1998, *ApJ*, 497, 800
- Kuan, Y.-J., Mehringer, D. M., & Snyder, L. E. 1996, *ApJ*, 459, 619
- Kurtz, S., Churchwell, E., & Wood, D. O. S. 1994, *ApJS*, 91, 659
- Ladd, E. F., Deane, J. R., Sanders, D. B., & Wynn-Williams, C. G. 1993, *ApJ*, 419, 186
- Lockett, P., & Elitzur, M. 1992, *ApJ*, 399, 704
- Mangum, J. G., Wootten, A., & Mundy, L. G. 1992, *ApJ*, 388, 467
- Martinez, A., Bujarrabal, V., & Alcolea, J. 1988, *A&AS*, 74, 273
- Menten, K. M. 1991, *ApJ*, 380, L75

- Menten, K. M., & Reid, M. J. 1995, *ApJ*, 445, L157
- Menten, K. M., & van der Tak, F. F. S. 2004, *A&A*, 414, 289, astro-ph/0310630
- Mitchell, G. F., Lee, S. W., Maillard, J.-P., Matthews, H., Hasegawa, T. I., & Harris, A. I.
1995, *ApJ*, 438, 794
- Morita, K.-I., Hasegawa, T., Ukita, N., Okumura, S. K., & Ishiguro, M. 1992, *PASJ*, 44, 373
- Neckel, T. 1978, *A&A*, 69, 51
- Olofsson, H., Hjalmarsen, A., & Rydbeck, O. E. H. 1981, *A&A*, 100, L30
- Padin, S. et al. 1989, *ApJ*, 337, L45
- Pardo, J. R., Alcolea, J., Bujarrabal, V., Colomer, F., del Romero, A., & de Vicente, P.
2004, *A&A*, 424, 145
- Peretto, N., André, P., & Belloche, A. 2006, *A&A*, 445, 979, astro-ph/0508619
- Plambeck, R. L., & Menten, K. M. 1990, *ApJ*, 364, 555
- Reid, M. J., Menten, K. M., Greenhill, L. J., & Chandler, C. J. 2007, *ApJ*, 664, 950,
arXiv:0704.2309
- Reid, M. J., Schneps, M. H., Moran, J. M., Gwinn, C. R., Genzel, R., Downes, D., &
Roennaeng, B. 1988, *ApJ*, 330, 809
- Rudolph, A., Welch, W. J., Palmer, P., & Dubrulle, B. 1990, *ApJ*, 363, 528
- Sandell, G. 2000, *A&A*, 358, 242
- Schneps, M. H., Moran, J. M., Genzel, R., Reid, M. J., Lane, A. P., & Downes, D. 1981,
ApJ, 249, 124

- Schreyer, K., Henning, T., van der Tak, F. F. S., Boonman, A. M. S., & van Dishoeck, E. F. 2002, *A&A*, 394, 561
- Schreyer, K., Semenov, D., Henning, T., & Forbrich, J. 2006, *ApJ*, 637, L129, arXiv:astro-ph/0601270
- Shepherd, D. S., Borders, T., Claussen, M., Shirley, Y., & Kurtz, S. 2004, *ApJ*, 614, 211, astro-ph/0406383
- Shepherd, D. S., Testi, L., & Stark, D. P. 2003, *ApJ*, 584, 882, astro-ph/0210555
- Snell, R. L., Scoville, N. Z., Sanders, D. B., & Erickson, N. R. 1984, *ApJ*, 284, 176
- Snyder, L. E., & Buhl, D. 1974, *ApJ*, 189, L31+
- Sridharan, T. K., Beuther, H., Schilke, P., Menten, K. M., & Wyrowski, F. 2002, *ApJ*, 566, 931, astro-ph/0110363
- Thaddeus, P., Mather, J., Davis, J. H., & Blair, G. N. 1974, *ApJ*, 192, L33+
- Torrelles, J. M., Gomez, J. F., Rodriguez, L. F., Ho, P. T. P., Curiel, S., & Vazquez, R. 1997, *ApJ*, 489, 744
- Trinidad, M. A. et al. 2003, *ApJ*, 589, 386
- Trinidad, M. A., Curiel, S., Torrelles, J. M., Rodríguez, L. F., Migenes, V., & Patel, N. 2006, *AJ*, 132, 1918
- Tsuboi, M., Ohta, E., Kasuga, T., Murata, Y., & Handa, T. 1996, *ApJ*, 461, L107+
- Ukita, N., Hasegawa, T., Kaifu, N., Morita, K. I., Okumura, S., Suzuki, H., Ohishi, M., & Hayashi, M. 1987, in *IAU Symp. 115: Star Forming Regions*, ed. M. Peimbert & J. Jugaku, 178–+

- van der Tak, F. F. S., & Menten, K. M. 2005, *A&A*, 437, 947, astro-ph/0504026
- van der Tak, F. F. S., Tuthill, P. G., & Danchi, W. C. 2005, *A&A*, 431, 993, astro-ph/0411142
- van der Tak, F. F. S., van Dishoeck, E. F., Evans, II, N. J., Bakker, E. J., & Blake, G. A. 1999, *ApJ*, 522, 991, astro-ph/9905035
- van der Tak, F. F. S., van Dishoeck, E. F., Evans, II, N. J., & Blake, G. A. 2000, *ApJ*, 537, 283, astro-ph/0001527
- Vogel, S. N., Genzel, R., & Palmer, P. 1987, *ApJ*, 316, 243
- Werner, M. W., Becklin, E. E., Gatley, I., Matthews, K., Neugebauer, G., & Wynn-Williams, C. G. 1979, *MNRAS*, 188, 463
- Willner, S. P. et al. 1982, *ApJ*, 253, 174
- Wilner, D. J., Reid, M. J., & Menten, K. M. 1999, *ApJ*, 513, 775
- Wilner, D. J., Welch, W. J., & Forster, J. R. 1995, *ApJ*, 449, L73+
- Wilson, T. L., Johnston, K. J., & Mauersberger, R. 1991, *A&A*, 251, 220
- Woody, D. P., Scott, S. L., Scoville, N. Z., Mundy, L. G., Sargent, A. I., Padin, S., Tinney, C. G., & Wilson, C. D. 1989, *ApJ*, 337, L41
- Wright, M. M., Gray, M. D., & Diamond, P. J. 2004, *MNRAS*, 350, 1253
- Wynn-Williams, C. G., Becklin, E. E., & Neugebauer, G. 1974, *ApJ*, 187, 473
- Zapata, L. A., Rodríguez, L. F., Ho, P. T. P., Beuther, H., & Zhang, Q. 2006, *AJ*, 131, 939, astro-ph/0510761
- Zavagno, A., Deharveng, L., Nadeau, D., & Caplan, J. 2002, *A&A*, 394, 225

Zhang, Q., & Ho, P. T. P. 1997, ApJ, 488, 241

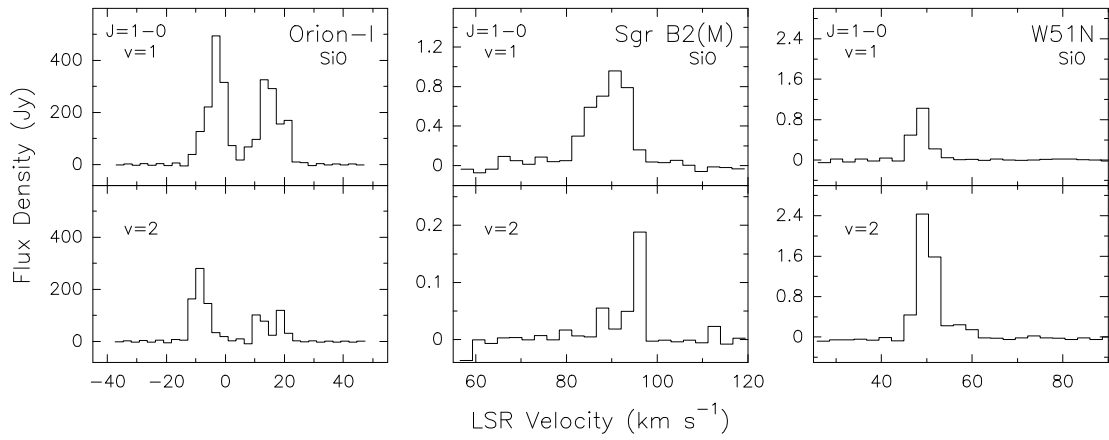


Fig. 1.— Spectra of the SiO $J = 1 - 0$, $v=1$ lines (top) and $v = 2$ lines (bottom) observed toward Source-I (left), Sgr B2(M) (middle), and W51N (right). The spectral resolution is 2.72 km s^{-1} .

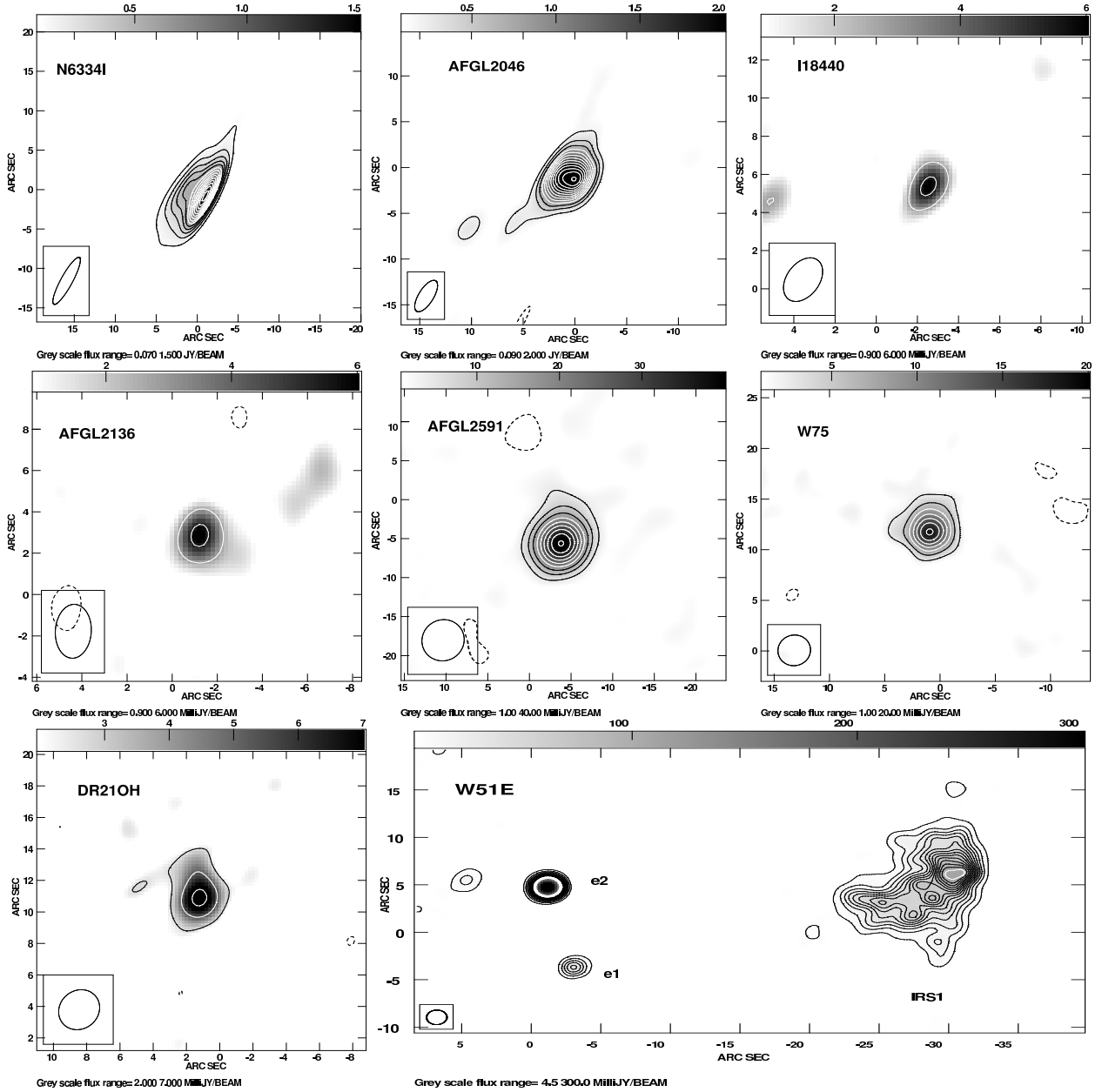


Fig. 2.— VLA 7mm continuum images. The half-power contour of the synthesized beam is shown in the bottom left corner of each image. The contours for the most of the sources are -5%, 5%, 10%, 15%, 20%, 25%, 30%, 35%, 40%, 45%, 50%, 55%, 60%, 65%, 70%, 75%, 80%, 90% and 95% the peak flux shown in Table 4. The var scale on the top of each image gives approximately the 7 mm peak continuum emission, and the range and units are indicated in the bottom part. The x and y coordinates in each sub-image are offsets (in arcsec) in right ascension and declination direction, respectively, from the positions listed in Table 1. The continuum images of Sgr B2(M) and W51N were made by averaging only the free-line

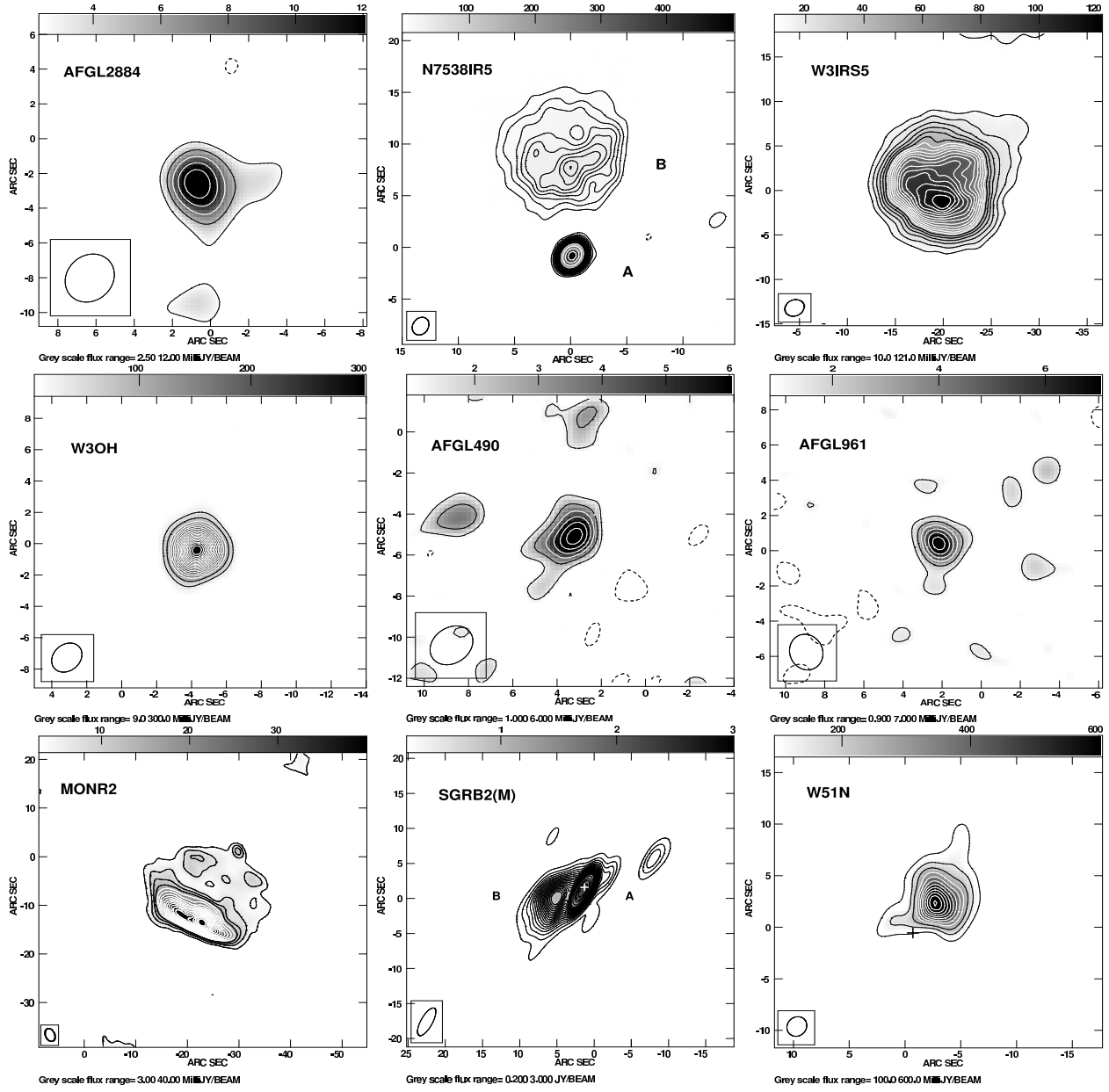


Fig. 2.— Continuation.

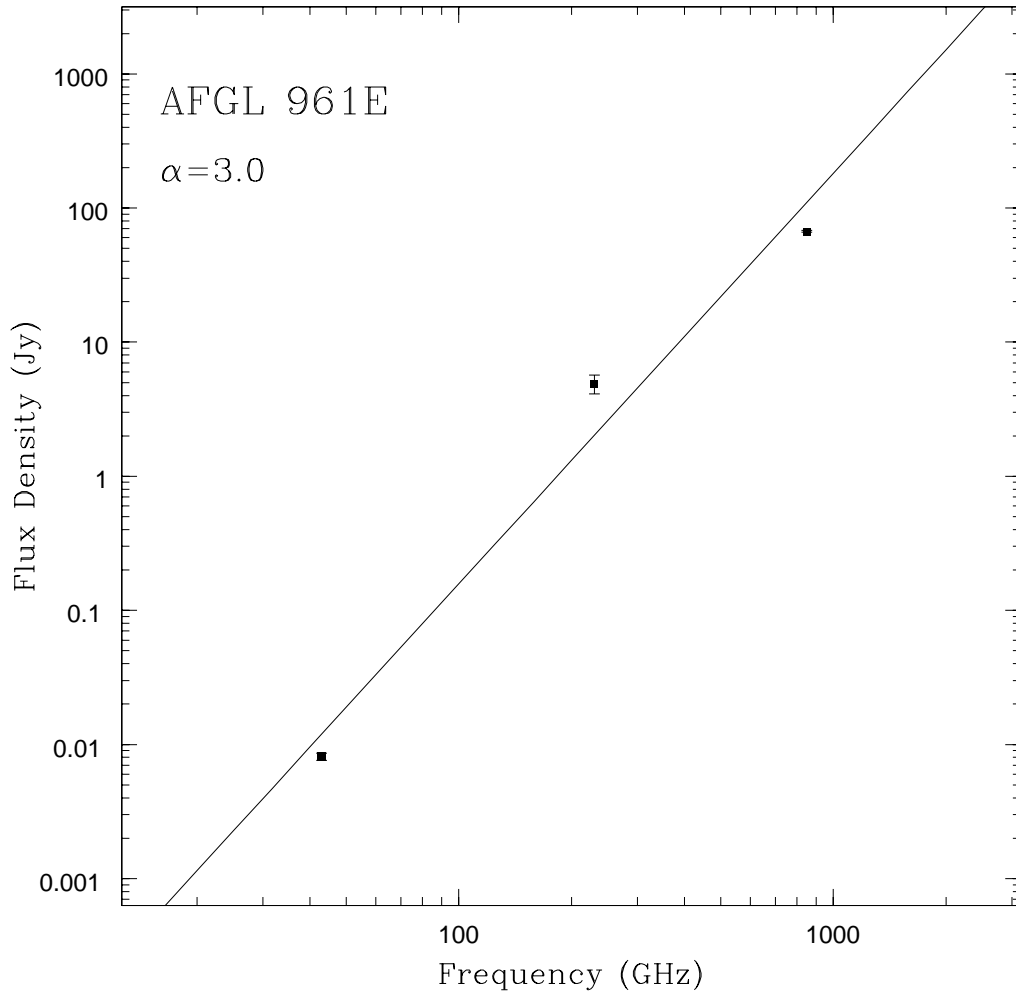


Fig. 3.— Spectral energy distribution of the source AFGL 961E combining data obtained with the VLA (7 mm, this paper) and millimeter telescopes (Guertler et al. 1991)). The line is a least-squares power-law fit of the form ($S_\nu \propto \nu^\alpha$) to the spectrum.

Table 1. Physical Parameters of Our Sample and SiO and Continuum Emission Results

Source	Coordinates		Physical Parameters			ΔS_M (mJy)	ΔS_C (mJy)	Ref.
	α_{2000} [<i>h m s</i>]	δ_{2000} [<i>° ' ''</i>]	D (kpc)	L_{bol} (L_{\odot})	M (M_{\odot})			
N6334I	17 20 53.50	-35 47 01.0	1.7	2.6×10^5	200	140	I	1,2
N6334I-N	17 20 54.60	-35 45 08.0	1.7	1.9×10^3	400	140	10	1,2
Sgr B2(M)	17 47 20.00	-28 23 05.0	7.1	1×10^6	500	D	I	3,29
AFGL 2046	18 00 30.40	-24 03 60.0	4.0	7×10^5	30	340	I	4
I18426–0204	18 45 12.80	-02 01 12.0	1.1	6.31×10^2	36	80	I	5,6
AFGL 7009S	18 34 19.70	-05 59 44.0	3.0	2.9×10^4	–	30	I	25
I18437–0216	18 46 22.70	-02 13 24.0	–	–	–	40	10	5,6
I18440–0148	18 46 36.30	-01 45 23.0	–	–	–	40	D	5,6
AFGL 2059	18 04 53.60	-24 26 42.0	1.5	1.6×10^4	–	40	3	14
I18102–1800	18 13 12.20	-17 59 35.0	2.6	6.3×10^4	413	40	3	5,6
G12.890+0.48	18 11 51.30	-17 31 29.0	3.6	3.2×10^4	1200	50	3	5,6
I18090–1832	18 12 01.90	-18 31 56.0	6.6	1.2×10^4	1011	50	3	5,6
W33 A	18 14 39.90	-17 51 59.0	4.0	1×10^5	1089	50	3	11,13,14
I18223–1243	18 25 10.90	-12 42 17.0	3.7	1.6×10^4	527	40	3	5,6
I18151–1208	18 17 57.10	-12 07 22.0	–	–	–	80	3	5,6
I18159–1550	18 18 47.30	-15 48 58.0	4.7	1.5×10^4	393	80	3	5,6
I18182–1433	18 21 07.90	-14 31 53.0	4.5	2×10^4	1507	60	3	5,6
AFGL 2136	18 22 26.50	-13 30 15.0	2.0	7×10^4	–	40	I	14
I18306–0835	18 33 21.80	-08 33 38.0	4.9	1.3×10^4	1721	40	3	5,6
W51N	19 23 40.10	14 31 06.0	7	2.8×10^6	1000	D	I	15,16,17
W51E	19 23 44.00	14 30 30.0	7	–	–	40	I	15,16,17
I19266+1745	19 28 54.00	17 51 56.0	0.3	5×10^1	3	30	10	5,6
I19220+1432	19 24 19.70	14 38 03.0	–	–	–	30	10	5,6
I19410+2258	19 43 11.40	23 44 06.0	2.1	1×10^4	418	30	3	5,6
I19411+2306	19 43 18.10	23 13 59.0	2.9	5×10^3	245	20	3	5,6
I19471+2641	19 49 09.90	26 48 52.0	–	–	–	40	4	5,6
NGC 6820	19 42 27.90	23 05 15.0	2.4	6.3×10^3	65	30	2	5,6
I19413+2306	19 43 28.90	23 40 04.0	1.8	2×10^2	115	30	10	5,6
I20051+3435	20 07 03.80	34 44 35.0	1.6	2×10^2	48	60	4	5,6
I20081+2720	20 10 11.50	27 29 06.0	–	–	–	40	4	5,6

Table 1—Continued

Source	Coordinates		Physical Parameters			ΔS_M (mJy)	ΔS_C (mJy)	Ref.
	α_{2000} [h m s]	δ_{2000} [° ′ ″]	D (kpc)	L_{bol} (L_\odot)	M (M_\odot)			
I20126+4104	20 14 26.00	41 13 32.0	–	–	–	20	3	5,6
I20205+3948	20 22 21.90	39 58 05.0	–	–	–	40	3	5,6
CPM 35	20 23 23.80	41 17 40.0	1.7	1.9×10^2	171	30	3	5,6
AFGL 2591	20 29 24.90	40 11 21.0	1.0	2×10^4	42	30	I	14
I20293+3952	20 31 10.70	40 03 10.0	1.3	2×10^3	98	30	4	5,6
I20319+3958	20 33 49.30	40 08 45.0	–	–	–	30	4	5,6
I20332+4124	20 35 00.50	41 34 48.0	–	–	–	20	4	5,6
I20343+4129	20 36 07.10	41 40 01.0	–	–	–	30	8	5,6
W75 N	20 38 36.40	42 37 22.0	2.0	a few $\times 10^5$	–	30	I	18
DR21(OH)	20 39 00.90	42 22 38.0	3.0	1×10^3	350	20	I	12,13
I22134+5834	22 15 09.10	58 49 09.0	–	–	–	20	4	5,6
AFGL 2884	22 19 18.10	63 18 49.0	0.9	–	–	20	I	28
I22551+6221	22 57 05.20	62 37 44.0	–	–	–	20	4	5,6
I22570+5912	22 59 06.50	59 28 49.0	–	–	–	30	4	5,6
I23033+5951	23 05 25.70	60 08 08.0	–	–	–	30	4	5,6
NGC 7538 IRS1	23 13 45.40	61 28 11.0	2.8	1.3×10^5	815	30	I	9,10,13
NGC 7538 IRS9	23 14 01.70	61 27 20.0	2.8	4.0×10^4	430	30	4	9,10,13
G111.25	23 16 09.30	59 55 23.0	4.8	2.0×10^4	–	30	4	27
I23151+5912	23 17 21.00	59 28 28.0	–	–	–	40	3	5,6
I23545+6508	23 57 05.20	65 25 11.0	–	–	–	40	3	5,6
W3 IRS5	02 25 40.70	62 05 52.0	2.2	1.7×10^5	262	60	I	7,8,13
W3(OH)	02 27 04.50	61 52 25.0	2.0	1×10^5	50	30	I	21
AFGL 490	03 27 38.40	58 47 05.0	1.0	$2.2\text{--}4.0 \times 10^3$	490	30	I	20
S255	06 12 54.90	17 59 23.0	2.5	6×10^4	–	40	3	23
G192.16	05 58 13.90	16 31 60.0	2.0	1×10^3	–	50	3	26
ORION-I	05 35 14.50	-05 22 30.0	0.41	$\sim 10^5$	–	D	16	19
I05358+3543	05 39 10.40	35 45 19.0	–	–	–	40	3	5,6
I05490+2658	05 52 12.90	26 59 33.0	–	–	–	40	3	5,6
AFGL 989	06 41 10.00	09 29 19.0	0.8	2×10^3	–	50	3	22
AFGL 961	06 34 37.60	04 12 44.0	1.6	8.9×10^3	–	20	I	24

Table 1—Continued

Source	Coordinates		Physical Parameters			ΔS_M (mJy)	ΔS_C (mJy)	Ref.
	α_{2000} [<i>h m s</i>]	δ_{2000} [<i>° ' ''</i>]	D (kpc)	L_{bol} (L_\odot)	M (M_\odot)			
MonR2	06 07 47.80	-06 22 55.0	1.0	1.3×10^4	–	30	I	14

Note. — The first column gives the source designation. **I** as first character in a source name stands for IRAS. Second and third column give right ascension and declination (J2000), respectively. Forth column lists the distance where the near kinematic distance is taken for sources discussed in refs. 5 and 6. Fifth and sixth columns the bolometric luminosity of the region containing the source and M the mass of its surrounding molecular core, respectively. Seventh column: ΔS_M is 4 times the rms noise in a single 2.72 km s^{-1} wide spectral channel. The noise levels of the $v = 1$ and 2 data cubes were very similar. **D** indicates that maser emission was detected (see Table 3 and Figure 1). Eighth column: ΔS_C is 4 times the rms noise of the continuum images. **I** indicates that continuum emission was detected and imaged (for these sources, see Table 4 and Figure 2). References are listed in the ninth column. They are: 1: Sandell (2000); 2: Neckel (1978); 3: Reid et al. (1988); 4: Gómez et al. (1991) and references therein; 5: Beuther et al. (2002); 6: Sridharan et al. (2002); 7: Ladd et al. (1993); 8: Humphreys (1978); 9: Werner et al. (1979); 10: Crampton et al. (1978); 11: Guertler et al. (1991); 12: van der Tak et al. (1999); 13: van der Tak et al. (2000); 14: Boonman & van Dishoeck (2003) and references therein; 15: Schneps et al. (1981); 16: Erickson & Tokunaga (1980); 17: Rudolph et al. (1990); 18: Torrelles et al. (1997); 19: Menten & Reid (1995); 20: Schreyer et al. (2002); 21: Wright et al. (2004) and references therein; 22: Peretto et al. (2006) and references therein; 23: Alvarez & Hoare (2005) and references therein; 24: Klein et al. (2005); 25: Zavagno et al. (2002); 26:

Shepherd et al. (2004); 27: Trinidad et al. (2006) and references therein; 28:
Kurtz et al. (1994); 29: de Vicente et al. (2000)

Table 2. Parameters of the Phase Calibrators

Calibrator	Phase Center		Bootstrapped	Synthesized Beam	
	α_{2000}	δ_{2000}	Flux Density	Size	P.A.
	[$^{\circ}$ $'$ $''$]	[$^{\circ}$ $'$ $''$]	[Jy]	[arcsec]	[deg.]
1717-337	17 17 36.03	-33 42 08.7	8.9	5.44×1.46	-25.3
1733-130	17 33 02.70	-13 04 49.5	7.9	2.53×1.62	-22.5
1833-210	18 33 39.91	-21 03 40.0	16.2	2.48×1.42	-11.7
1851+005	18 51 46.72	00 35 32.4	1.8	2.03×1.60	-30.0
1832-105	18 32 20.83	-10 35 11.2	2.0	1.99×1.44	-1.60
1743-038	17 43 58.85	-03 50 04.6	6.6	2.13×1.47	-23.8
1925+211	19 25 59.60	21 06 26.1	2.1	1.47×1.34	0.0
2015+371	20 15 28.73	37 10 59.5	3.8	1.51×1.42	-45.3
22250+558	22 50 42.85	55 50 14.5	1.1	1.63×1.43	-29.3
0228+673	02 28 50.05	67 21 03.0	5.2	1.89×1.42	-49.0
0613+131	06 13 57.69	13 06 45.4	1.7	1.57×1.48	-3.4
0541-056	05 41 38.08	-05 41 49.4	1.5	1.92×1.49	0.3
0555+398	05 55 30.80	39 48 49.1	3.5	1.54×1.38	-10.6

Note. — Positional accuracy is estimated to be $0.01''$

Table 3. Properties of the Detected Maser Emission

Source	Peak Position		Line	S_p (Jy beam ⁻¹)	v_p (km s ⁻¹)	$\int S dv$ (Jy km s ⁻¹)	v -range (km s ⁻¹)	L_ν (s ⁻¹)
	α_{2000}	δ_{2000}						
	[^h ^m ^s]	[[°] ' ^{''}]						
Source-I ^a	05 35 14.507	-05 22 30.47	$v = 1$	490	-3	6463(35)	[-13, 23]	6.7×10^{44}
	05 35 14.505	-05 22 30.42	$v = 2$	279	-8	2712(26)	[-13, 23]	2.8×10^{44}
Sgr B2(M)	17 47 20.098	-28 23 03.40	$v = 1$	0.93	91	8.8(0.4)	[81, 98]	3.4×10^{44}
	17 47 20.095	-28 23 03.53	$v = 2$	0.19	96	0.88(0.08)	[\approx 79, 98]	3.4×10^{43}
W51N	19 23 40.055	14 31 05.51	$v = 1$	1.0	49	5.1(0.1)	[45, 56]	1.5×10^{44}
	19 23 40.052	14 31 05.45	$v = 2$	2.5	49	15(0.1)	[45, 61]	4.4×10^{44}
Miras			$v = 1$					a few $\times 10^{43}$
			$v = 2$					a few $\times 10^{43}$
RSGs			$v = 1$					10^{44} – 10^{46}
			$v = 2$					10^{44} – 10^{46}

Note. — Measured values are given for the SiO $J = 1 - 0$, $v = 1$ and $v = 2$ lines. S_p is the flux density at the velocity of peak emission, v_p . $\int S dv$ is flux density integrated over the v -range showing emission. L_ν is the isotropic luminosity in units of photons per second. For the 43.3 GHz SiO $J = 1 - 0$ lines $L_\nu = 10^{44}$ s⁻¹ corresponds to a luminosity of $7.5 \times 10^{-6} L_\odot$.

Note. — Positional accuracy is estimated to be 0.01''

^aThe peak position corresponds to the blueshifted integrated emission and the redshifted peak position is $\alpha[J2000]=05^h35^m14.500^s$ and $\delta[J2000]=-05^\circ22'30.36''$ for $v = 1$ and $v = 2$.

Table 4. Parameters of the 43.3 GHz Continuum Sources

Source	Peak Position		Density	Peak	Deconvolved Parameters	
	α_{2000}	δ_{2000}	Flux	Flux	Size	P.A.
	[$^{\circ}$ $'$ $''$]	[$^{\circ}$ $'$ $''$]	[mJy]	[mJy Beam $^{-1}$]	[arcsec 2]	[deg.]
N6334I	17 20 53.428	-35 47 01.60	2300	1400	5.7×2.6	-32.0
Sgr B2(M)-A	17 47 20.121	-28 23 03.90	3600	2600	2.1×1.2	146
Sgr B2(M)-B	17 47 20.380	-28 23 05.00	3200	1800	2.7×2.5	144
AFGL 2046	18 00 30.442	-24 04 01.21	7600	2700	3.0×2.7	84
I18440	18 46 36.132	-01 45 17.61	5.5	6.4	-	-
AFGL 2136	18 22 26.409	-13 30 12.25	7.4	5.7	-	-
W51N	19 23 39.917	14 31 09.19	3800	624	3.9×2.9	20
W51e2	19 23 43.918	14 30 34.70	391	390	-	-
W51e1	19 23 43.786	14 30 26.32	42	39	-	-
W51IRS1	19 23 41.913	14 30 36.23	747	182	3.4×1.9	157
AFGL 2591	20 29 24.545	40 11 15.06	50	40	1.9×1.1	79
W75N-VLA3Bb	20 38 36.475	42 37 33.93	24	18	2.1×1.1	174
DR21(OH)	20 39 01.027	42 22 49.23	16	6.9	3.0×1.3	2.8
AFGL 2884	22 19 18.169	63 18 46.31	20	15	2.1×0.5	38
NGC 7538 IRS1-A	23 13 45.381	61 28 10.18	530	530	-	-
NGC 7538 IRS1-B	61 28 18.806	23 13 45.39	710	82	4.5×4.2	153
W3 IRS5	02 25 37.900	62 05 50.48	520	160	-	-
W3(OH)	02 27 03.887	61 52 24.54	1500	866	-	-
AFGL 490	03 27 38.834	58 46 59.95	9.8	8.2	-	-
AFGL 961	06 34 37.743	04 12 44.43	8.1	7.9	-	-
MonR2	06 07 46.270	-06 23 08.55	940	730	-	-

Note. — Those parameters were determined from a linearized least-squares fit to a Gaussian ellipsoid function using the AIPS task IMFIT. Sources with failed deconvolved fitting are indicated with the sign '-'.

Note. — Positional accuracy is estimated to be 0.01''

Table 5. Nature of the 42 GHz Continuum Emission

Name	Nature	References
N6334I	UC HII region (NGC 6334F)	Carral et al. (2002)
Sgr B2(M)	Cluster of HII regions	Gaume et al. (1995);de Pree et al. (1996) de Pree et al. (1998)
AFGL 2046	UC HII region (G5.89-0.39)	Gómez et al. (1991)
IRAS 18440	UC HII region?	Here
AFGL 2136	UC HII region? (RS4)	Menten & van der Tak (2004)
W51N	UC HII region(W51-IRS2/d2/d1)	Gaume et al. (1993);Zhang & Ho (1997)
W51-e2	UC HII region	Gaume et al. (1993);Zhang & Ho (1997)
W51-e1	UC HII region	Gaume et al. (1993);Zhang & Ho (1997)
W51-IRS1	Compact HII region	Gaume et al. (1993);Zhang & Ho (1997)
AFGL 2591	UC HII region (VLA1)/Ionized thermal jet	Trinidad et al. (2003); van der Tak et al. (2005)
W75 North	Ionized thermal jet (VLA3-Bb)	Shepherd et al. (2003)
DR21(OH)	Dusty Core (MM1)	Here
AFGL 2884	Ionized stellar wind?(S140 IRS 1)	Hoare (2002);Hoare (2006)
N7538-IRS1-A	UCHII Variable	Franco-Hernández & Rodríguez (2004); Here; Wynn-Williams et al. (1974)
N7538-IRS1-B	Compact HII region	Wynn-Williams et al. (1974); Here
W3 IRS5	UC HII region	Menten & van der Tak (2004)
W3(OH)	UC HII region	Wilner et al. (1999)
AFGL 490	Circumstellar Disk/Envelope	Chini et al. (1991);Henning et al. (1990); Schreyer et al. (2006)
AFGL 961E	Dusty Core?	Here
MONR2	Compact HII region	Here